Numerical Simulation of Nonadiabatic Electron Excitation in the Strong-Field Regime. 3. Polyacene Neutrals and Cations

Stanley M. Smith,[†] Xiaosong Li,[‡] Alexei Markevitch,[§,⊥] Dmitri Romanov,[||,⊥] Robert J. Levis,[§,⊥] and H. Bernhard Schlegel*[,†]

Department of Chemistry, Wayne State University, Detroit, Michigan 48202, Department of Chemistry, University of Washington, Seattle, Washington 98195, Departments of Chemistry and Physics, Center for Advanced Photonics Research, Temple University, Philadelphia, Pennsylvania 19122

Received: January 16, 2007; In Final Form: May 22, 2007

The electron optical response for a series of linear polyacenes and their molecular ions (mono and dications) in strong laser fields was studied using time-dependent Hartree−Fock theory. The interactions of benzene, naphthalene, anthracene, and tetracene with pulsed fields at a frequency of 1.55 eV and intensities of 8.77×10^{13}, 3.07×10^{13}, 1.23×10^{13}, and 2.75×10^{12} W/cm^2, respectively, were calculated using the 6-31G(d,p) basis set. Nonadiabatic processes, including nonadiabatic time evolution of the dipole moment, Löwden charges, and occupation numbers, were studied. The nonadiabatic response increased with the length of the molecule and was greatest for the molecular monocations. The only exception was tetracene, in which the very strong response of the dication was due to a near resonance with the applied field. The intensity and frequency dependence of the dipole moment response for the monocations of naphthalene and anthracene was also calculated. As the intensity increased, the population of higher-energy excited-states increased, and as the frequency increased, the excitation volume increased in good agreement with the Dykhne approximation.

I. Introduction

Nonadiabatic effects are prominent in many photophysical processes including vision,[1,2] intersystem crossing,[3−6] and many photochemical reactions.[7−12] When a molecule interacts with a strong laser field, nonadiabatic effects not only contribute but may dominate the interaction. Thus, to study nonadiabatic effects, both theoretically and experimentally, it is necessary to achieve coherent control of nonadiabatic processes. The simulation and analysis of the dynamics of short, intense laser pulses interacting with large conjugated molecules will help in the understanding of these processes.

Intense laser fields can cause a variety of nonperturbative phenomena termed strong-field effects. These phenomena can be divided into two types, those that require knowledge of the electron dynamics and those that require knowledge of coupled electron−nuclear dynamics. Some examples of the first type include field tunneling and barrier suppression ionization,[13−16] above threshold ionization (ATI),[17−19] higher-order harmonic generation,[20−24] and nonadiabatic multielectron dynamics (NMED).[25−28] Examples of coupled electron−nuclear dynamics include above-threshold dissociation,[29,30] bond softening and hardening,[29−31] charge-resonance enhanced ionization,[32,33] Coulomb explosions,[34−37] and nonadiabatic charge localization.[37] Thus, knowledge of the dynamics of the electronic wave function is essential for understanding these processes. The goal of the present paper is to model the nonadiabatic response of polyacene molecules prior to ionization.

Atomic systems have been studied extensively, whereas the study of molecular strong-field processes is far from complete. Keldysh[13] showed that multiphoton ionization (MPI) and tunnel ionization (TI) can be distinguished using the adiabaticity parameter (γ), which is the ratio of the laser frequency and characteristic tunneling frequency. The underlying physics of the Keldysh treatment was developed further by Faisal[38] and Reiss.[39] The two most commonly used extensions to Keldysh-Faisal-Reiss (KFR) theory are Perelomov, Popov, and Terent'ev[40] (PPT) theory and Ammosov, Delone, and Krainov[14] (ADK) theory. An extension to ADK theory has been made for small molecules (MO-ADK[41]). However, for larger molecules this semiphenomenological theory becomes impracticable.

Intense laser dissociation and ionization processes have been reported for conjugated polyatomic molecules such as benzene, naphthalene, anthracene, hexatriene, octatetraene, decatetraene, and C_{60}.[15,16,25−28,42−46] The response of these molecules to a nonresonant laser field is mainly determined by the first-order polarizability and transition dipole moment matrix elements. Nonlinear processes can also contribute through higher-order polarizabilities. These properties have been extensively studied for linear polyenes[47−56] and selected polyacenes and their molecular cations.[54,57] At high intensities, a nonadiabatic multielectron dynamics approach can be used to predict fragmentation probabilities. This approach was successfully used to predict the fragmentation probabilities for a series of polyacenes ranging from benzene to tetracene.[27,28] The approach assumes ionization occurs prior to fragmentation. Thus, electron dynamics for neutral molecules as well as their molecular ions is necessary to describe the observed experimental results.

Bandrauk[33,58−66] and collaborators have used full electron−nuclear wavepacket dynamics to study the ionization of H_2 in intense laser fields. Mukamel[67,68] and co-workers have simulated π electron dynamics in octatetraene with a semiempirical

* To whom correspondence should be addressed. E-mail: hbs@chem.wayne.edu.
[†] Wayne State University.
[‡] University of Washington.
[§] Department of Chemistry, Temple University.
[||] Department of Physics, Temple University.
[⊥] Center for Advanced Photonics Research, Temple University.

10.1021/jp070380b CCC: $37.00
Published on Web 07/11/2007

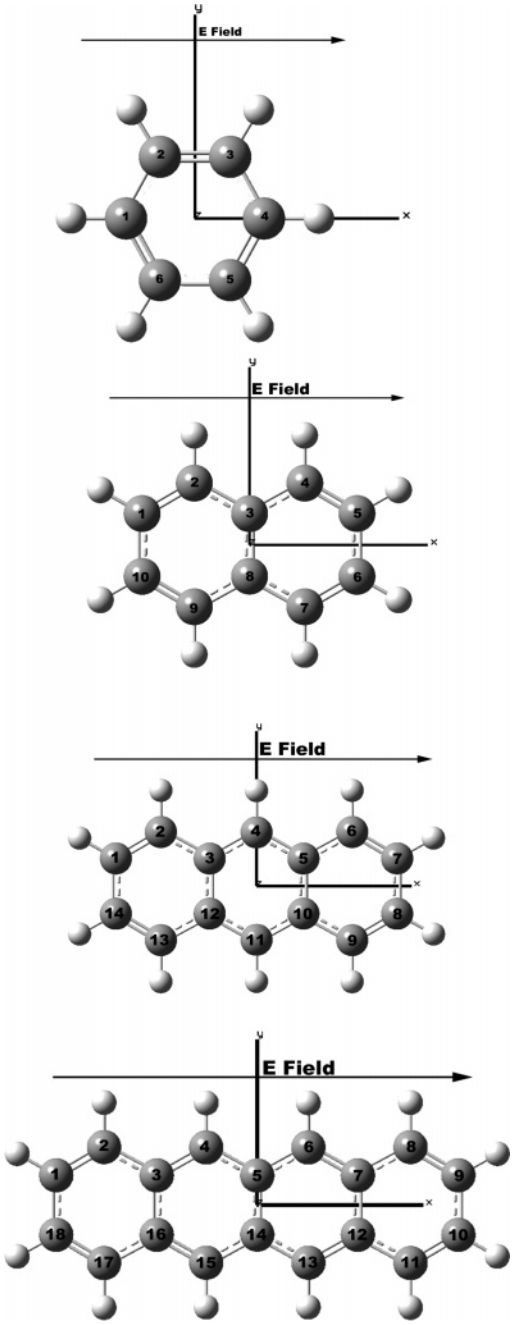

Figure 1. The electric field orientation for benzene, naphthalene, anthracene, and tetracene.

Hamiltonian and have modeled ionization saturation intensities in a multielectron system in a finite one-dimensional box. Chu et al.[69−75] have studied the many electron atoms and diatomics using time-dependent pseudospectral methods, self-interaction corrected density functional theory, and Floquet matrix techniques. Klamroth, Saalfrank, and co-workers[76−78] have used time-dependent configuration interaction with single excitations (TD−CIS) to simulate dipole switching in lithium cyanide and have employed TD−CIS and optimal control theory to shape short, intense pulses for state-selective excitation of *N*-methylquinoline. We have compared TD−CIS and time-dependent Hartree−Fock (TDHF) treatments for polyenes in short, intense laser pulses and have found good agreement provided that the degree of nonadiabatic excitation remained small.[79] Cederbaum[80,81] and collaborators have used a multielectron wavepacket dynamics approach to investigate hole migration following ionization.

TABLE 1: The Field Free Excited-States of Benzene, Naphthalene, Anthracene, and Tetracene Calculated Using Linear Response TDHF at the Indicated Geometry and Charge State

main transitions[a] (TDHF coefficient)	energy (eV) from TDHF	oscillator strength	Fourier coefficient[b]
Benzene Neutral			
HOMO − 1 → LUMO (0.51)	8.00	0.69	1.3
HOMO − 1 → LUMO + 1 (0.52)	8.00	0.72	1.3
Benzene 1+ Neutral Geometry			
HOMO −1 → LUMO (0.66)	2.46	0.01	17.1
SOMO → LUMO (0.71)	5.39	0.22	3.5
HOMO → LUMO + 1 (0.61)	8.24	0.07	3.0
Benzene 1+ Ion Geometry			
SOMO → HOMO (1.00)	1.80	0.001	2.4
HOMO → SOMO (0.75)	2.82	0.003	6.2
HOMO → LUMO + 1 (0.70)	3.52	0.016	2.8
HOMO −2 → SOMO (0.95)	5.01	0.001	3.4
SOMO → LUMO (0.67)	5.60	0.228	
HOMO −3 → LUMO (0.88)	6.14	0.001	2.0
SOMO → LUMO + 1 (0.82)	8.72	0.39	13.0
Benzene 2+ Neutral Geometry			
HOMO − 1 → LUMO (0.70)	4.93	0.27	11.4
HOMO → LUMO 1+ (0.70)	7.53	0.35	
Butadiene 2+ Ion Geometry			
HOMO −2 → LUMO (0.70)	4.06	0.00	
HOMO − 1 → LUMO + 1 (0.71)	5.35	0.30	10.8
HOMO → LUMO + 2 (0.70)	7.41	0.38	0.2
HOMO → LUMO + 3 (0.69)	8.56	0.33	0.3
Naphthalene Neutral			
HOMO → LUMO + 1 (0.51)	6.94	1.54	1.4
Naphthalene 1+ Neutral Geometry			
HOMO → SOMO (0.89)	1.49	0.10	29.5
SOMO → LUMO (0.66)	4.42	0.20	3.7
HOMO → LUMO (0.49)	5.45	0.15	2.2
LUMO → HOMO + 1 (0.60)	6.98	0.52	6.0
Naphthalene 1+ Ion Geometry			
HOMO → SOMO (0.98)	2.05	0.08	22.2
SOMO → LUMO (0.92)	3.86	0.23	7.9
SOMO → LUMO + 1 (0.58)	6.13	0.30	1.6
HOMO − 1 → LUMO (0.79)	7.26	0.98	3.3
Naphthalene 2+ Neutral Geometry			
HOMO − 1 → LUMO (0.70)	2.85	0.34	21.6
HOMO → LUMO + 1 (0.68)	6.63	0.90	0.4
Naphthalene 2+ Ion Geometry			
HOMO − 1 → LUMO (0.71)	3.64	0.25	10.3
HOMO → LUMO + 1 (0.68)	6.35	0.88	2.1
Anthracene Neutral			
HOMO − 1 → LUMO (0.51)	4.69	0.01	
HOMO − 1 → LUMO + 1 (0.51)	6.21	2.42	5.3
HOMO − 3 → LUMO + 3 (0.60)	11.94	0.12	
HOMO − 6 → LUMO + 6 (0.41)	13.89	0.02	0.1
Anthracene 1+ Neutral Geometry			
HOMO → SOMO (0.96)	1.96	0.32	26.4
HOMO → LUMO (0.91)	3.10	0.50	9.9
HOMO − 1 → LUMO + 1 (0.43)	6.81	0.02	5.4
Anthracene 2+ Neutral Geometry			
HOMO → LUMO (0.69)	2.49	0.51	12.2
HOMO − 1 → LUMO + 1 (0.68)	5.94	1.46	3.5
HOMO − 3 → LUMO + 2 (0.54)	9.28	0.06	0.7
Tetracene Neutral			
HOMO → LUMO + 1 (0.52)	5.70	3.34	0.99
Tetracene 1+ Neutral Geometry			
HOMO → SOMO (1.10)	0.71	0.29	46.0
SOMO → LUMO (0.60)	2.42	0.04	12.5
HOMO → LUMO (0.42)	3.95	0.31	9.4
HOMO → LUMO + 2 (0.46)	5.29	0.01	8.5
Tetracene 2+ Neutral Geometry			
HOMO → LUMO (0.69)	2.22	0.81	133
HOMO − 4 → LUMO (0.69)	4.97	0.03	23.6
HOMO −1 → LUMO + 1 (0.66)	8.69	0.20	3.9

[a] Excitation energies were calculated using linear response TDHF theory with the 6-31G(d,p) basis set. [b] $\omega = 1.55$ eV.

TABLE 2: Polarizabilities (Å^3) of the Benzene, Naphthalene, Anthracene, and Tetracene Calculated at the Indicated Level of Theory, Charge State, and Geometry

	benzene			naphthalene		
	0	1+	2+	0	1+	2+
Neutral Optimized Geometry						
static $\alpha(0)$ (in au)						
HF/6-31G(d,p)	67.68	69.81	76.01	143.0	242.4	176.4
PBE0/6-31G(d,p)[a]	69.11	71.51	70.00	149.4	173.5	163.5
dynamic $\alpha(\omega)$ $\omega = 760$ nm (in au)						
HF/6-31G(d,p)	69.09	73.94	79.94	147.8	547.7	211.7
PBE0/6-31G(d,p)[a]	70.62	75.84	73.61	155.2	259.7	187.1
Cation Optimized Geometry						
static $\alpha(0)$ (in au)						
HF/6-31G(d,p)		69.00	68.11		190.8	157.6
PBE0/6-31G(d,p)[a]		69.70	66.24		167.6	157.6
dynamic $\alpha(\omega)$ $\omega = 760$ nm (in au)						
HF/6-31G(d,p)		71.74	70.30		279.2	172.1
PBE0/6-31G(d,p)[a]		72.96	68.26		205.9	171.4
	anthracene			tetracene		
	0	1+	2+	0	1+	2+
Neutral Optimized Geometry						
static $\alpha(0)$ (in au)						
UHF/6-31G(d,p)	242.0	369.3	373.4	362.9	605.3	647.1
PBE0/6-31G(d,p)[a]				396.5	546.9	583.7
dynamic $\alpha(\omega)$ $\omega = 760$ nm (in au)						
UHF/6-31G(d,p)	253.3	689.6	521.5	384.8	2039.7	1094.7
PBE0/6-31G(d,p)[a]				427.9	−7513.8	986.9

[a] Polarizabilities were calculated at the HF or UHF/6-31G(d,p) geometries.

TABLE 3: Calculated Ionization Probabilities Using the Nonadiabatic Multielectron Excitation and Tunnel Ionization Theories

molecule	excited-state energy (Δ) (eV)	transition dipole moment (au)	NME ionization probability[a]	tunnel ionization probability[b]
		Benzene		
neutral	8.00	1.87	0.0022	0.11
1+ neutral geometry	5.39	1.03	0.0052	3.1×10^{-5}
1+ ion geometry	5.60	1.12	0.0054	1.1×10^{-4}
2+ neutral geometry	7.53	1.37	0.00034	5.5×10^{-9}
2+ ion geometry	7.41	1.25	0.00023	
		Naphthalene		
neutral	6.94	3.01	0.0001	0.11
1+ neutral geometry	6.99	1.71	0.011	6×10^{-6}
1+ ion geometry	7.26	2.34	0.00018	4×10^{-5}
2+ neutral geometry	6.63	2.35	0.00025	1.29×10^{-12}
2+ ion geometry	6.35	2.37	0.00026	
		Anthracene		
neutral	6.21	3.99	0.00015	0.0078
1+ neutral geometry	6.37	2.75	0.00047	6.7×10^{-7}
2+ neutral geometry	5.94	3.17	0.00056	8.8×10^{-18}
		Tetracene		
neutral	5.70	4.88	0.00006	4.5×10^{-8}
1+ neutral geometry	6.28	3.39	0.0011	9.8×10^{-20}
2+ neutral geometry	5.44	3.90	0.00095	7.1×10^{-31}

[a] Calculated using the NME theory of ref 27. [b] Calculated using the ADK-type theory of ref 95.

Recently, we reported that TDHF[82] theory provides a good approximation to the electronic optical response of a series of linear polyenes[83] and their molecular cations[84] in strong laser fields. These simulations showed that (a) the coupling of the molecule to the field increased with length for neutral molecules, (b) the coupling was greater for molecular ions than for neutral molecules, and (c) the instantaneous dipole moment and charge distribution respond nonadiabatically for larger molecules and stronger fields. There were also residual oscillations in the instantaneous dipole moment after the pulsed field returned to zero that can be interpreted as nonresonant nonadiabatic excitations. Fourier analysis of the residual oscillations revealed that the lowest excited-states dominate these oscillations.

The success of the TDHF simulations for polyenes indicates that this same approach should work on the polyacenes in the present study. The computational techniques are briefly described in the methodology section. Experimental results for the polyacene series show that 1+ molecular cations are produced at laser field intensities of 1.1×10^{14}, 4.1×10^{13}, 2.1×10^{13}, and 4.5×10^{12} W/cm^2 for benzene, naphthalene, anthracene, and tetracene, respectively.[27] The experimental pulse duration was ~65 fs full-width at half-maximum (fwhm) at $\lambda = 760$ nm. Our simulations for the polyacenes were carried out with a pulse duration of ~4.5 fs fwhm at $\lambda = 760$ nm ($\omega = 0.06$ au) and field strengths of 0.050, 0.0296, 0.0187, and 0.00885 au, which corresponds to intensities of 8.77×10^{13},

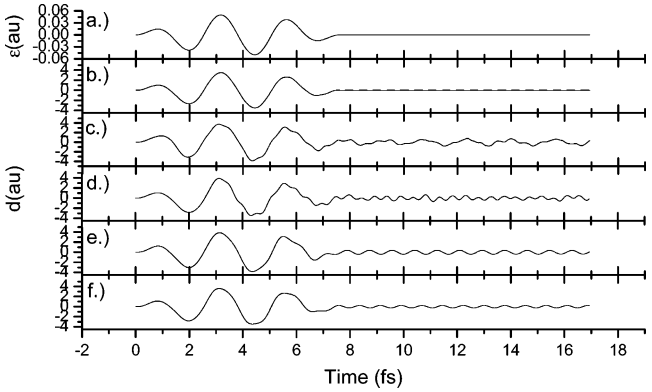

Figure 2. The electric field (a) and dipole moment response for benzene neutral (b), 1+ ion at the neutral geometry (c), 1+ at the ion geometry (d), 2+ ion at the neutral geometry (e), and 2+ at the ion geometry (f) for $\omega = 1.55$ eV and $\mathbf{E}_{max} = 0.050$ au.

3.07×10^{13}, 1.23×10^{13}, and 2.75×10^{12} W/cm^2, respectively. These intensities are 60−80% of the experimental intensities where production of molecular monocations was observed.

In the first section of Results and Discussion, we use nonadiabatic multielectron excitation theory[27,28] to verify that no significant ionization takes place for the intensities, frequencies, and pulse durations used in our simulations. In the next sections we investigate the effects of short, intense pulses on the electron dynamics of a series of polyacenes and their cations. There are two possibilities for the laser−molecule interaction after ionization: (i) the laser pulse can interact with the molecule immediately after ionization so that the geometry is near the neutral geometry, or (ii) sufficient time can elapse for the geometry to relax. As the molecules increase in size, the change in geometry should have less effect on the polarizability and electron dynamics. Hence, only the geometries of the 1+ and 2+ molecular cations for benzene and naphthalene were optimized. Because the intensity for each molecule is different, comparisons should only be made among different charge states of the same molecule and not between molecules. In the last two sections we examine the effects of field strength and frequency on the response of naphthalene and anthracene monocations.

II. Methodology

The TDHF equations can be used to describe the interactions of light with molecules.[20,58−63,82,85−92] The TDHF equations in an orthonormal basis can be written in terms of the Fock matrix (**F**) and the one-electron density matrix (**P**).

$$i\frac{\mathrm{d}\mathbf{P}(t_i)}{\mathrm{d}t} = [\mathbf{F}(t_i), \mathbf{P}(t_i)] \tag{1}$$

An efficient method for integrating the TD−HF equations has been described in previous papers.[82,83] The Fock matrix depends on time not only because of the electric field of the laser (**E**(t)) but also because of the time-dependence of the electron density. To simulate a short pulse, |**E**(t)| is increased linearly to |$\mathbf{E}_{max}$| at the end of the first cycle, remains at |$\mathbf{E}_{max}$| for one cycle, and then decreases linearly to zero by the end of the next cycle.

$$\mathbf{E}(t) = (\omega t/2\pi)\mathbf{E}_{max} \quad \text{for } 0 \le t \le 2\pi/\omega$$
$$\mathbf{E}(t) = \mathbf{E}_{max} \quad \text{for } 2\pi/\omega \le t \le 4\pi/\omega$$
$$\mathbf{E}(t) = (3 - \omega t/2\pi)\mathbf{E}_{max} \quad \text{for } 4\pi/\omega \le t \le 6\pi/\omega$$
$$\mathbf{E}(t) = 0 \quad \text{for } t < 0 \text{ and } t > 6\pi/\omega \tag{2}$$

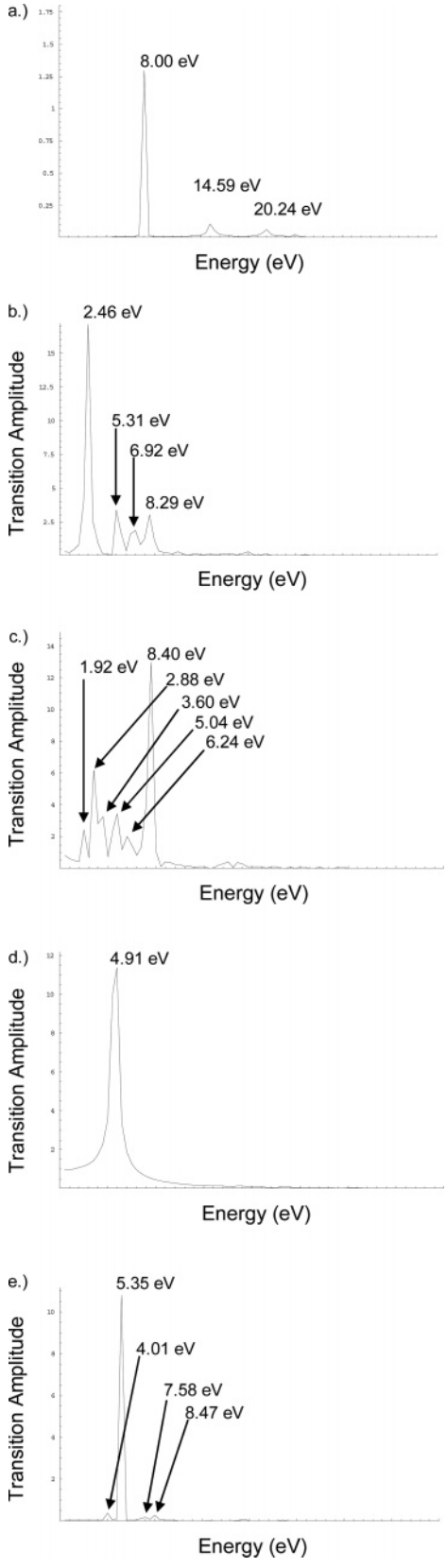

Figure 3. The Fourier transforms of the residual dipole moment oscillations for benzene neutral (a), benzene 1+ at the neutral geometry (b), benzene 1+ at the ion geometry (c), benzene 2+ at the neutral geometry (d), and benzene 1+ at the ion geometry for $\omega = 1.55$ eV and $\mathbf{E}_{max} = 0.050$ au.

The response of a molecule to an intense field can be described by several useful properties. The effective charge on atom A

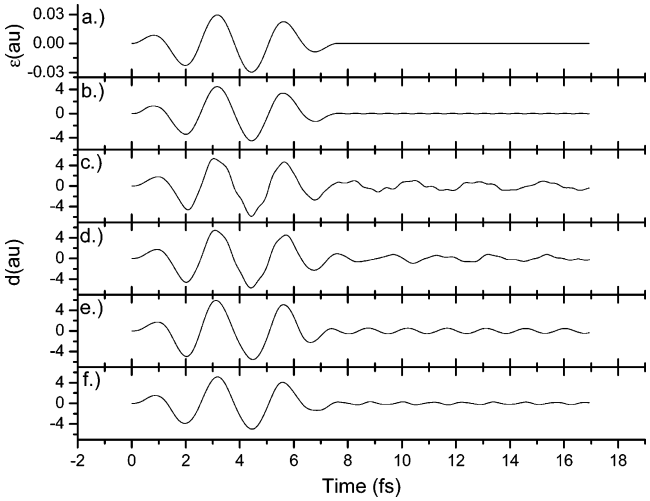

Figure 4. The electric field (a) and dipole moment response for naphthalene neutral (b), 1+ ion at the neutral geometry (c), 1+ at the ion geometry (d), 2+ ion at the neutral geometry (e), and 2+ at the ion geometry (f) for $\omega = 1.55$ eV and $\mathbf{E}_{max} = 0.0296$ au.

can be computed using Löwdin population analysis

$$q_A = Z_A - \sum_{i \subset A} P_{ii}(t) \tag{3}$$

where Z_A is the charge on the nucleus, P_{ii} are the diagonal elements of the density matrix in the orthonormal basis, and the sum is over basis functions on atom A. Orbital occupation numbers can also be obtained by projecting the time-dependent density matrix onto the initial, field-free orbitals

$$n_k(t_i) = \mathbf{C}_k^T(0)\, \mathbf{P}(t_i)\, \mathbf{C}_k\,(0) \tag{4}$$

where $\mathbf{C}_k(0)$ is the kth eigenvector of the converged Fock matrix at $t = 0$. The instantaneous dipole moment is given by eq 5

$$\mu(t_i) = \sum_A Z_A \mathbf{R}_A - tr(\mathbf{D}'\mathbf{P}'(t_i)) \tag{5}$$

where $\mathbf{D}'$ are the dipole moment integrals in the atomic orbital (AO) basis. For the purpose of analysis, it is also useful to write the components of the dipole in terms of the polarizability (α) and the first, second, and higher hyperpolarizabilities (β, γ, etc.);

$$\mu_i = \mu_i^0 + \sum_j \alpha_{ij} E_j + \frac{1}{2}\sum_{jk} \beta_{ijk} E_j E_k + \frac{1}{6}\sum_{jkl} \gamma_{ijkl} E_j E_k E_l + \ldots \tag{6}$$

The β values are small for benzene, naphthalene, anthracene, and tetracene, mainly due to symmetry. As such, they do not contribute significantly for the polyacenes in the present study.

Electronic dynamics in a field were simulated using the development version of the GAUSSIAN[93] series of programs with the addition of the unitary transform TDHF algorithm (UT−TDHF). Calculations were performed at the HF/6-31G-(d,p) level of theory with a step size of 0.0012 fs (0.05 au). Because continuum functions are not included in the basis set, these simulations are intended only to model the response prior to ionization and not the ionization process itself. For each of the molecules, the integrations were carried out for 16 fs. The geometry and electric field direction are shown in Figure 1. Field parameters varied for each molecule. $|\mathbf{E}_{max}| = 0.05$ au (8.77×10^{13} W/cm^2), 0.02959 au (3.07×10^{13} W/cm^2), 0.01873 au (1.23×10^{13} W/cm^2), and 0.00885 au (2.75×10^{12} W/cm^2)

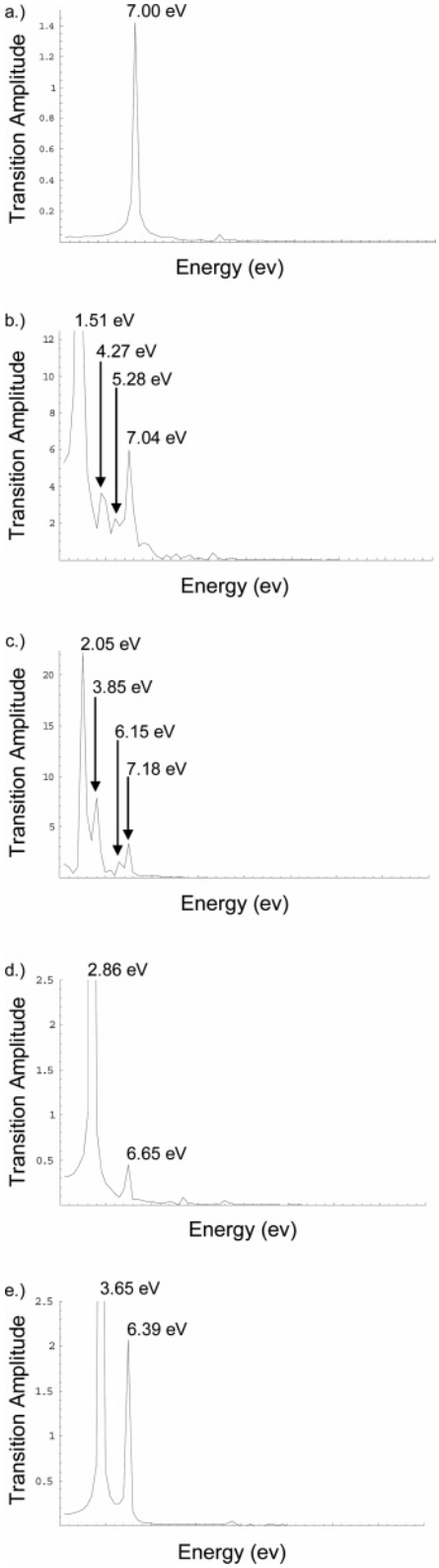

Figure 5. The Fourier transforms of the residual dipole moment oscillations for naphthalene neutral (a), naphthalene 1+ at the neutral geometry (b), naphthalene 1+ at the ion geometry (c), naphthalene 2+ at the neutral geometry (d), and naphthalene 1+ at the ion geometry (e) for $\omega = 1.55$ eV and $\mathbf{E}_{max} = 0.0296$ au.

for benzene, naphthalene, anthracene, and tetracene, respectively, and $\omega = 0.06$ au (760 nm) for each molecule. The intensity dependence was studied for naphthalene 1+ and anthracene 1+, both at the neutral geometry. The field parameters for naphthalene monocation were $\omega = 1.55$ eV and $\mathbf{E}_{max} = 0.0155$,

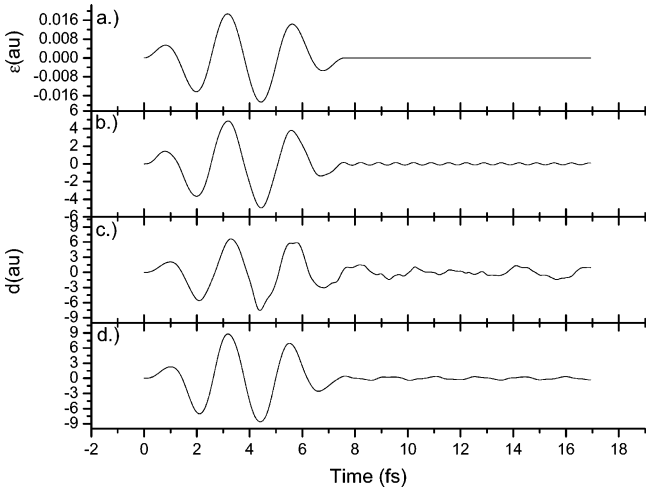

Figure 6. The electric field (a) and dipole moment response for anthracene neutral (b), 1+ ion at the neutral geometry (c), and 2+ at the neutral geometry (d) for $\omega = 1.55$ eV and $\mathbf{E}_{max} = 0.0187$ au.

0.0298, and 0.0340 au, and the parameters for anthracene monocation were $\omega = 1.55$ eV with $\mathbf{E}_{max} = 0.0110$, 0.0184, and 0.0200 au. Likewise, the effect of field energy was also studied for both mocations at the neutral geometry. Field parameters used for napthtalene 1+ were $\mathbf{E}_{max} = 0.0155$ au, pulse duration $\sim$ 7 fs, and $\omega = 1.55$, 2.00, and 3.00 eV. For anthracene 1+ these parmeters were $\mathbf{E}_{max} = 0.0184$ au, pulse duration $\sim$ 7 fs, and $\omega = 1.00$, 2.00, and 3.00 eV. Integrations were started from the converged electronic ground states. The phase of the field φ was chosen to be zero, and the nuclei were not permitted to move during the calculation.

III. Results and Discussion

The TDHF simulations of the neutral molecules and the 1+ and 2+ molecular cations of benzene, naphthalene, anthracene, and tetracene were carried out using a transform-limited pulse so that a basic understanding of the electron dynamics could be gained. Nuclear movement was not permitted in this investigation. The response to shaped pulses and nuclear motion will be the subject of subsequent studies.[94] The response of the molecules to the laser field was probed using the instantaneous dipole moment, charge distribution, and orbital occupation numbers. Situations where the dipole moment or charge distribution did not exactly follow the field will be termed nonadiabatic behaviors or responses, and situations where the dipole moment and charges continue to oscillate after the field has returned to zero will be taken as a signal of nonadiabatic coupling or excitation. The simulations were done using a short pulse with fwhm $\sim$ 4.5 fs (ca $\sim$7 fs total pulse width) at the normal Ti:Sapphire laser frequency (0.06 au, 760 nm). This pulse type has been used previously and permits the study of the electron dynamics after the field has returned to zero. Fourier analysis of the dipole moment response after the field has returned to zero is an important tool in the study of the nonadiabatic coupling of the field free states.

The weak-field (adiabatic) response is primarily due to low lying states with significant oscillator strength. Table 1 shows the lowest energy field free excited-states with significant oscillator strength for each given molecule, geometry, and charge state calculated at the linear response TDHF level of theory (also known as the random phase approximation, RPA). In each instance, these states involve $\pi \rightarrow \pi^*$ transitions; however, these transition are not necessarily associated the lowest lying excited-state. For the purposes of simplicity, the

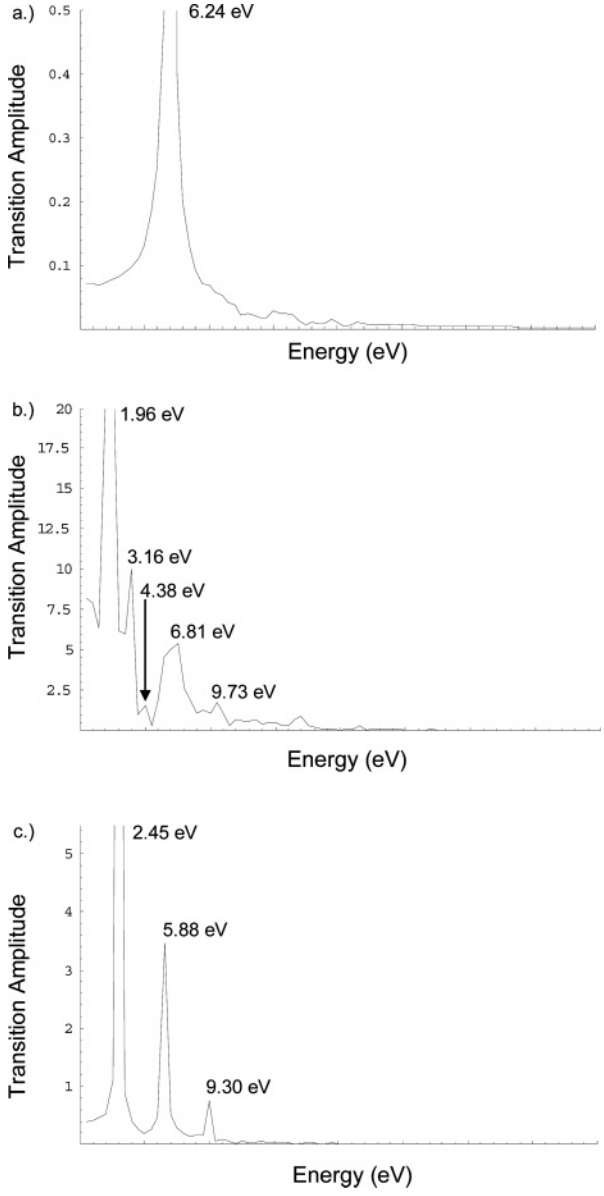

Figure 7. The Fourier transforms of the residual dipole moment oscillations for anthracene neutral (a), anthracene 1+ at the neutral geometry (b), and anthracene 2+ at the neutral geometry (c) for $\omega = 1.55$ eV and $\mathbf{E}_{max} = 0.0187$ au.

following common abbreviations will be used. Highest occupied molecular orbital (HOMO) and lowest unoccupied molecular orbital (LUMO) are the highest occupied and lowest unoccupied orbitals for the closed shell neutral molecules and 2+ molecular cations. For the open shell systems, 1+ molecular cations, the orbital with a single electron will be referred to as the singly occupied molecular orbital (SOMO), while the π orbital just below the SOMO is termed the HOMO and the π^* orbital directly above the SOMO is termed the LUMO. The static and dynamic polarizabilities for benzene, naphthalene, anthracene, and tetracene neutral molecules, 1+, and 2+ cations are shown in Table 2 for two levels of theory and for neutral and cation optimized geometries. The worst agreement between Hartree−Fock and density functional theory (PBE0) for the closed shell (neutral and 2+ ions) polarizability is 8% for benzene, 13% for naphthalene, 8% for anthracene, and 10% for tetracene. The agreement of the Hartree−Fock and density functional theory polarizabilities for the 1+ cations of naphthalene, anthracene, and tetracene is not as good. We have previously shown[83,84,102]

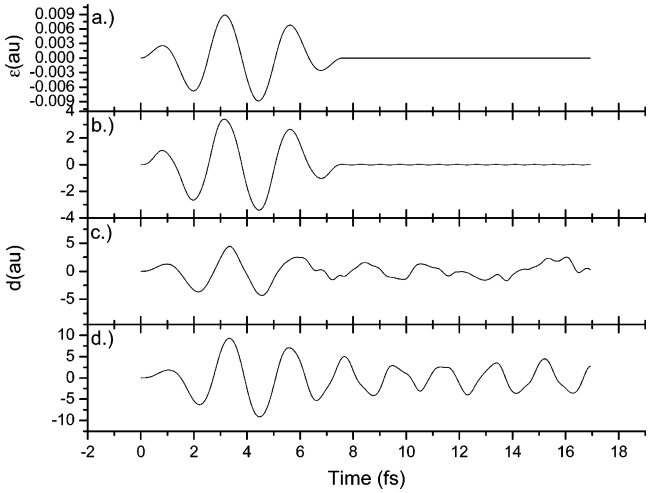

Figure 8. The electric field (a) and dipole moment response for tetracene neutral (b), 1+ ion at the neutral geometry (c), and 2+ at the neutral geometry (d) for $\omega = 1.55$ eV and $\mathbf{E}_{max} = 0.00885$ au.

that this is a result of spin contamination and not an effect of electron correlation. The difference between the HF and PBE0 dynamic polarizability for tetracene 1+ is due to an excited-state resonance with the applied electric field. This resonance is much more prominent at the PBE0 level of theory.

A. Ionization Probability. In our previous work,[27,28] we reported experimental laser intensities for these polyacenes that produce predominately molecular ions (using a 60 fs fwhm pulse). In this computational study we use much shorter 4.5 fs fwhm pulses, and we set the maximum laser intensity between 60 and 80% of the experimental laser intensities reported in ref 27. Under these conditions, NME theory is expected to accurately predict the ionization probabilities for these molecules; ADK-type tunnel ionization theory has also been used even though it tends to overestimate the ionization probabilities (see below).

The main features of NME theory are formation of a quasicontinuum (QC) of excited-states and excitation to the QC through a doorway state. The QC is formed as the strong laser field shifts and mixes the energy levels of the excited-state manifold, thus allowing electrons to rapidly climb up and ionize. The doorway state is the state that is most strongly coupled to the ground state. For each of the molecules in this study, the doorway state was shown to be the lowest energy charge-transfer state. As assumed in ref 27, excitation to the doorway state results in rapid ionization. NME theory equates excitation to ionization, thus it actually predicts the ionization probabilities as slightly higher than experimentally observed for the same pulse conditions in the simulation. The results of the NME calculation are listed in Table 3. It is apparent that, over the duration of the laser pulse and under the conditions of our simulations, NME predicts no significant ionization. The largest ionization probability is 0.011 for the naphthalene 1+ ion at the neutral geometry.

The last column of Table 3 shows the total integrated ionization probability using the ADK-type tunnel ionization method of Corkum[95] that, by comparison with experiment, may overestimate ionization probabilities for molecules[27,96−99] by more than an order of magnitude. A modification to this method for molecules by Brabec[100] does well for some molecules but unfortunately makes the assumption that polarizability decreases on ionization, which is not the case for the present molecules. The ionization probability is higher for some molecules using ADK tunnel ionization theory and is lower for others. The most

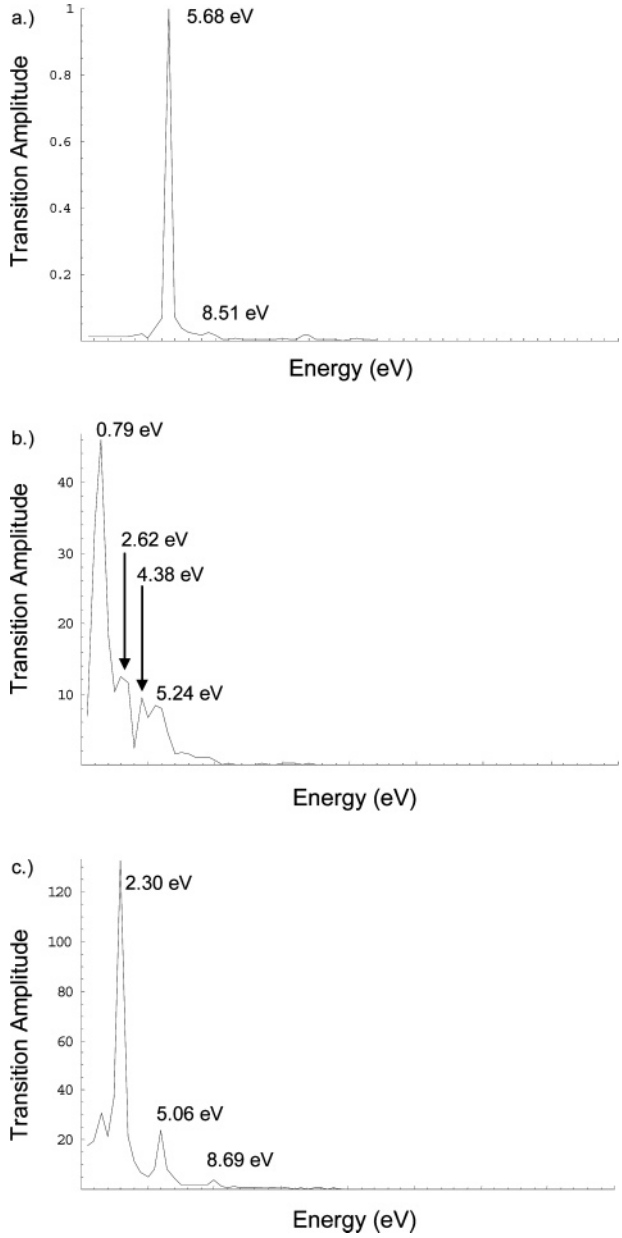

Figure 9. The Fourier transforms of the residual dipole moment oscillations for tetracene neutral (a), tetracene 1+ at the neutral geometry (b), and tetracene 2+ at the neutral geometry (c) for $\omega = 1.55$ eV and $\mathbf{E}_{max} = 0.00885$ au.

significant differences are for the neutral molecules of benzene and naphthalene, whose ionization probabilities are 0.11.

B. Benzene. Figure 2 shows the time evolution of the electric field (panel a) and the time evolution of the instantaneous dipole moment for neutral benzene (panel b), benzene 1+ at the neutral geometry (panel c), benzene 1+ at the ion geometry (panel d), benzene 2+ at the neutral geometry (panel e) and benzene 2+ at the ion geometry (panel f). For neutral benzene, the maximum dipole moment using TDHF and eq 5 is 3.51 au, whereas the dipole moment using eq 6 and the dynamic polarizability of 69.09 au (from Table 2) is 3.45 au. This same analysis for benzene 1+ and 2+ at the neutral geometry yields values of 3.61 and 3.69 au, and 3.89 and 4.00 au, respectively, for the dipole moment response from TDHF and eq 6. These all suggest that the higher-order processes do not contribute significantly to the dipole moment response for benzene and its 1+ and 2+ ions. Similar results are observed for benzene 1+ and 2+ cations evaluated at the ion geometry.

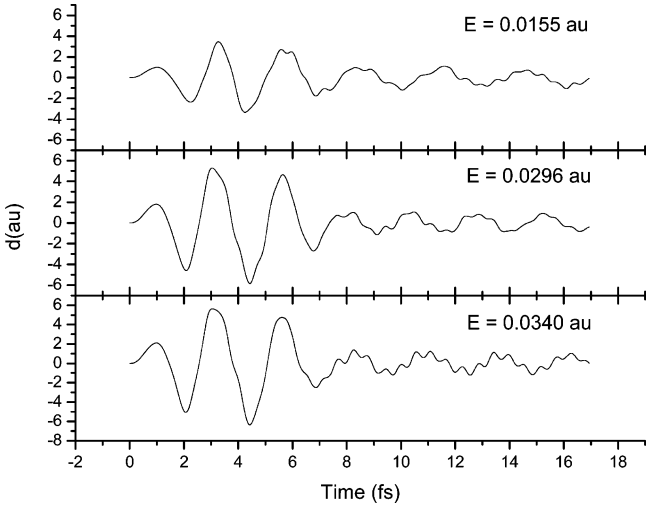

Figure 10. The dipole response of the naphthalene 1+ cation at the neutral geometry for electric field strengths of 0.0155, 0.0296, and 0.0340 au with $\omega = 1.55$ eV.

During the time the field is on, the instantaneous dipole moment appears to follow the field adiabatically for neutral benzene, whereas nonadiabatic character is evident for each of the ions (Figure 2, panels b−f). The greatest amount of nonadiabatic character is evident for the 1+ ions, indicating that they are probably the most strongly coupled to the field. After the field returns to zero, there are residual oscillations in the instantaneous dipole moment. Fourier analysis of these residual oscillations for each molecular geometry and charge state shows (see Figure 3) one main peak for the neutral and both 2+ ions, whereas there are several peaks for both of the 1+ ions. The main peaks correspond to excited energies of 8.00, 2.31, 2.88, 4.91, and 5.35 eV for neutral benzene, benzene 1+ at the neutral geometry, benzene 1+ at the ion geometry, benzene 2+ at the neutral geometry, and benzene 2+ at the ion geometry, respectively. These excited-states are all $\pi \rightarrow \pi^*$ transitions. The ratios of the Fourier coefficients (peak heights) corresponding to these energies with respect to the neutral benzene peak height are 1, 17, 13, 11, and 11 (see Table 1). These peak heights indicate that the 1+ ions are the most strongly coupled to the electric field. In addition to the largest Fourier coefficients, these two ions have several other peaks with Fourier coefficients up to $^1/_2$ the height of the largest peak. Thus, they have the greatest excitation volume, again indicating that they are the most strongly coupled to the field.

For benzene, the laser field is applied along the *x*-axis that connects two carbon atoms as shown in Figure 1. As a result, the two carbon atoms lying on the *x*-axis (C_1 and C_4) build up the largest charge separation, whereas carbons C_2 and C_5 have the same charge and carbons C_3 and C_6 have the same charge ($-C_2$ and $-C_5$). Each of the charge states and geometries for benzene follows this pattern; however, the magnitudes of the charges are different for different charge states.

C. Naphthalene. Figure 4 shows the time evolution of the electric field (panel a) and the time evolution of the instantaneous dipole moment for neutral naphthalene (panel b), naphthalene 1+ at the neutral geometry (panel c), naphthalene 1+ at the ion geometry (panel d), naphthalene 2+ at the neutral geometry (panel e), and naphthalene 2+ at the ion geometry (panel f). The instantaneous dipole moment appears to follow the field adiabatically for the neutral and both 2+ ions, whereas there is an obvious nonadiabatic character for both geometries for the 1+ ion. Fourier analysis of the residual dipole moment oscillations (see Figure 5) again shows mainly one peak for the closed shell systems and one main peak and several smaller peaks for the two open shell systems (i.e., both 1+ ions). The Fourier coefficients (peak heights) normalized to the naphthalene neutral coefficient are 1, 21, 16, 15, and 8 for the series (see Table 1). Again, the 1+ ions (21 and 16) are most strongly coupled to the field because they have the lowest field free excitation energies as determined from linear response TDHF (1.49 and 2.05 eV (see Table 1)). As a check, eq 6 can be used to calculate the initial coupling to the field. The 1+ cations have the largest polarizabilities, indicating that they should coupled most strongly to the field.

While the field is "on", the charge oscillation for neutral naphthalene is largest for end carbons (1, 10, 5, and 6 in Figure 1). When the field returns to zero, the magnitude of the residual charge oscillations is small and similar for all carbons. For the ions, when the field is "on", the time evolution of the charge oscillation is identical to the neutral molecule with end carbons exhibiting the largest charge localization. When the field is "off", the charge oscillations are quite different from the

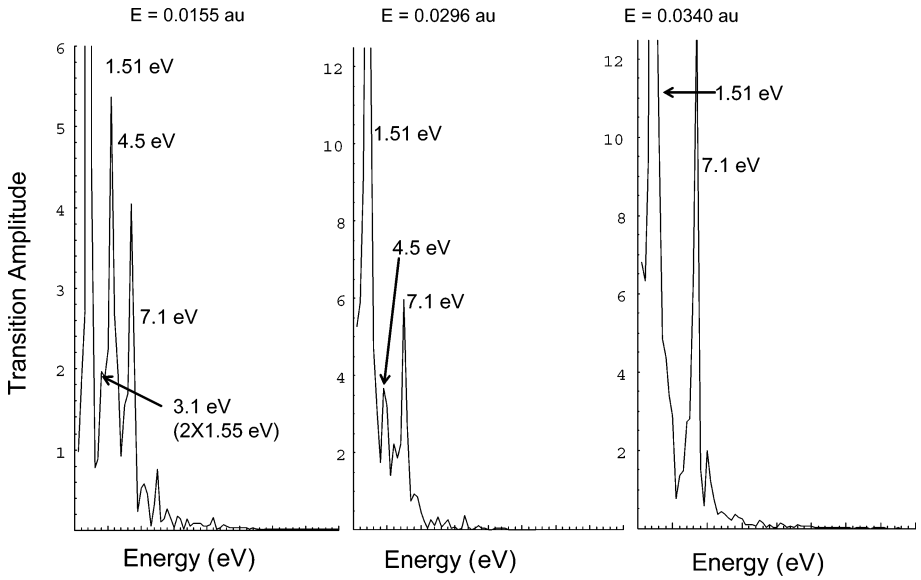

Figure 11. The Fourier transform of the residual dipole moment oscillations of naphthalene 1+ at the neutral geometry for electric field intensities of 0.0155, 0.0296, and 0.0340 au with $\omega = 1.55$ eV.

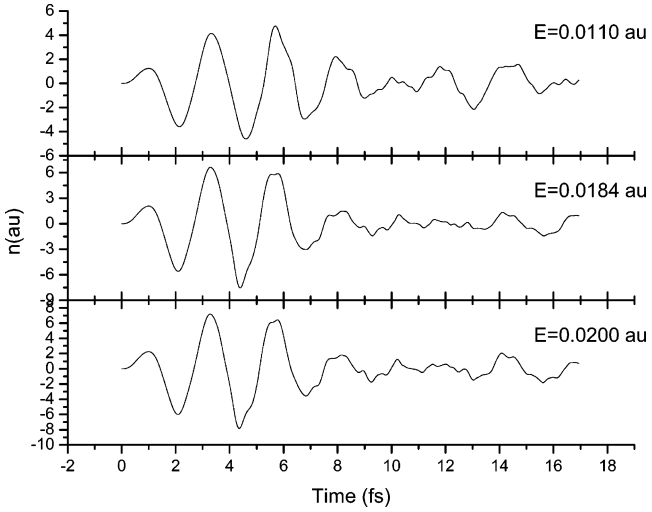

Figure 12. The dipole response of the anthracene 1+ cation at the neutral geometry for electric field strengths of 0.0110, 0.0184, and 0.0200 au $\omega = 1.55$ eV.

neutral molecule. The carbons adjacent to the end carbons (atoms 2, 9, 4, and 7 in Figure 1) have the largest charge localization. This can be understood in terms of the symmetry of the field free orbitals. On the time scale of the simulation, the amplitude of the charge oscillations for these carbons is nearly the same with the field on or off.

D. Anthracene. Figure 6 shows the time evolution of the electric field (panel a) and the time evolution of the instantaneous dipole moment for neutral anthracene (panel b), anthracene 1+ at the neutral geometry (panel c), and anthracene 2+ at the neutral geometry (panel d). Because geometry optimization is expected to have a smaller effect on the larger ions, the simulations were carried out only for the neutral geometries. Fourier analysis of the residual oscillations (see Figure 7) shows one main peak at 6.24 eV and a number of smaller higher-energy peaks (11.99 and 13.92 eV) associated with higher-energy $\pi \rightarrow \pi^*$ transitions. These agree very well with the values listed in Table 1. The time evolution of the charge distribution is very complex, and the largest charge localization is on the four carbons at each end of the molecule (atoms 1, 2, 13, 14, 6, 7, 8, and 9 in Figure 1).

E. Tetracene. The time evolution of the instantaneous dipole moment for the neutral molecule, the 1+ ion at the neutral geometry, and the 2+ ion at the neutral geometry is shown in Figure 8, panels b, c, and d, respectively. There appears to be little to no nonadiabatic character for the neutral molecule and the 2+ cation, whereas there appears to be slight nonadiabatic behavior for the 1+ cation. Fourier transformation of the residual dipole moment oscillation for all three molecules reveals several peaks for each molecule (see Figure 9). The neutral molecule has one main peak at 5.68 eV and three other very small peaks corresponding to higher-energy excited-states. The 1+ cation has a very complex Fourier transform. The main peak is at 0.79 eV with other smaller peaks at energies of 2.36, 3.93, 5.50, and 7.33 eV. These are all $\pi \rightarrow \pi^*$ transitions and correspond well with excited-states calculated using linear response TDHF. The Fourier transform of the 2+ cation shows several peaks, with the main peaks corresponding to energies of 2.30, 5.05, and 8.73 eV. The Fourier coefficient of the 2.30 eV peak of the 2+ cation is 2.9 times larger than the coefficient of the 2.36 eV peak of the 1+ cation and is 130 times larger than the coefficient of the 5.68 eV peak of the neutral molecule. The Fourier coefficient for the 2+ ion is the largest because it is associated with the lowest excited-state energy, and linear response TDHF shows a lower lying excited-state (1.58 eV) that is nearly resonant with the field (1.55 eV). Because there is no peak in the Fourier transform corresponding to this excited-state, excitation to this state from the ground state and from this state to higher lying excited-states must have occurred during the pulse. The time evolution of the charge distribution is very complex, and the largest charge localization is on atoms 1, 2, 17, 18, 8, 9, 10, and 11, as expected.

F. The Effects of Field Strength on the Electron Dynamics of Naphthalene 1+ and Anthracene 1+ Cations. Figure 10 shows the dipole moment response for naphthalene 1+ at the neutral geometry for electric field intensities of 0.015, 0.0296, and 0.0340 au with $\omega = 1.55$ eV. The differences in the dipole moment evolution are readily apparent. Nonadiabatic character can be seen for all of the field strengths. The residual dipole moment oscillations depend significantly on the field strength. The field strength increase leads to increases in the higher frequency components, as can be seen in the Fourier transform of the oscillations for each field strength (Figure 11). There are

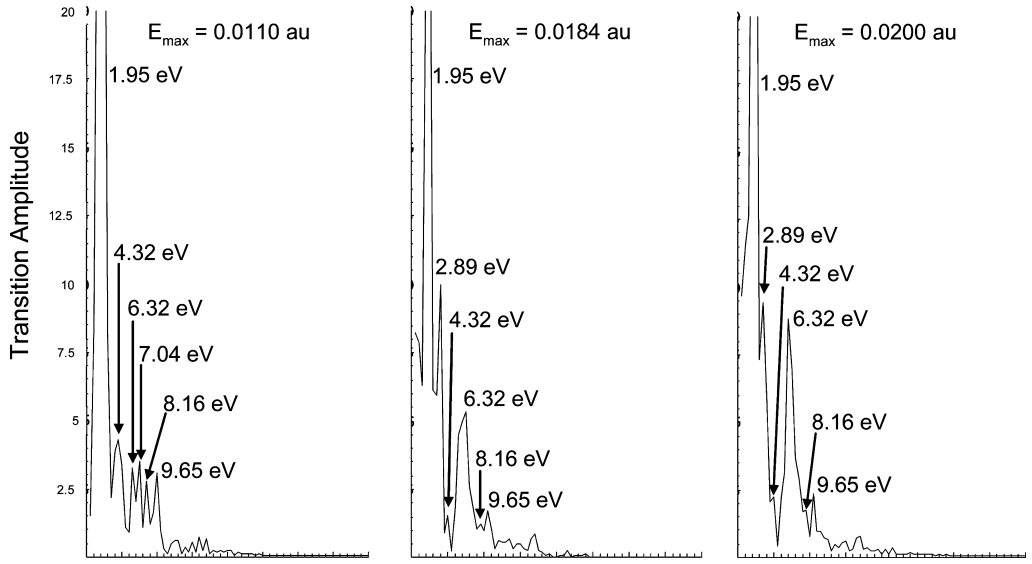

Figure 13. The Fourier transform of the residual dipole moment oscillations of anthracene 1+ at the neutral geometry for electric field intensities of 0.0110, 0.0184, and 0.0200 au $\omega = 1.55$ eV.

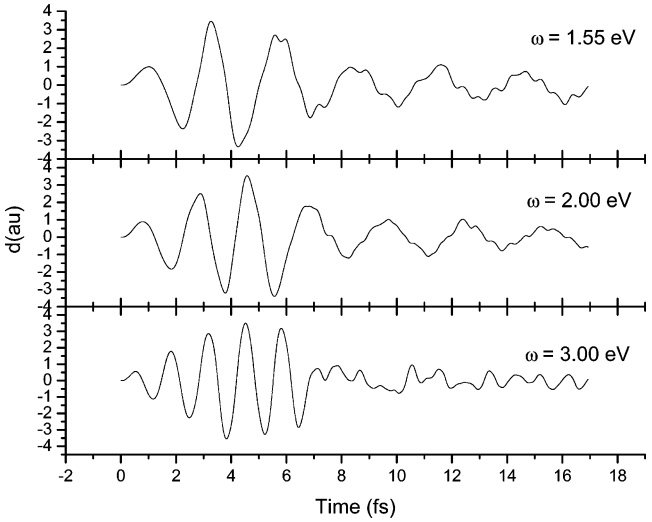

Figure 14. The dipole response of the naphthalene 1+ cation at the neutral geometry for electric field frequencies of 1.55, 2.00, and 3.00 eV for $\mathbf{E}_{max} = 0.0155$ au.

three main peaks at 1.51, 4.5, and 7.1 eV and a smaller peak at 10.8 eV. These peaks correspond to excited-states calculated at the linear response TDHF level of theory. The relative magnitudes of the Fourier coefficients of the 1.51 eV peaks are 1, 0.81, and 0.80 for field strengths of 0.0155, 0.0296, and 0.0340 au, respectively. Correspondingly, the relative magnitudes are 1, 0.68, and 0 for the 4.5 eV peak and 1, 1.47, and 3.30 for the 7.1 eV peak. This may suggest that the transition probability of the higher-energy 7.1 eV peak increases at the expense of the two lower lying peaks.

Figure 12 shows the time evolution of the dipole moment for anthracene 1+ at the neutral geometry for field strengths of 0.0110, 0.0184, and 0.0200 au, respectively. It is clear that anthracene 1+ responds very similarly to naphthalene 1+. Increasing the field strength increases the higher frequency components of the residual dipole moment oscillations. Figure 13 displays the Fourier transforms of the time evolutions shown in Figure 12 for the three field strengths. A comparison of the plots confirms that increasing the field strength increases the coefficients of the higher-energy states, most notably the 6.32 eV state.

These two examples for the naphthalene monocation and the anthracene monocation show interesting properties common to both molecules. Increasing the field strength increases the total excitation volume and the transition probability of some excited-states while decreasing the probability for other states. The increase in excitation volume is in qualitative agreement with published results from Landau−Zener and Dykhne type theories[25−28,101] that give the excitation probability over one laser half cycle. For a two-state system this is given by eq 7

$$P_{|g\rangle\rightarrow|DS\rangle} = \exp\left\{-\frac{\pi\Delta^2}{4\omega E_0 \mu}\right\} \quad (7)$$

where Δ is the energy difference between the two states, ω is the laser frequency, E_0 is the maximum magnitude of the electric field, and μ is the transition dipole moment between two states. Increasing the field strength increases the transition probability and thus the excitation volume.

G. The Effects of Field Frequency on the Electron Dynamics of Naphthalene 1+ and Anthracene 1+ Cations. Because changing the field intensity has significant effects on residual dipole moment oscillations, the effects of changing field frequency also need to be examined. Figure 14 shows the effects of three different field energies on the instantaneous dipole moment of the naphthalene 1+ cation. The field parameters are $\mathbf{E}_{max} = 0.0155$ au, pulse width ~ 7 fs, and $\omega = 1.55$, 2.00, and 3.00 eV. Here, the lowest field strength was chosen because it showed the most developed Fourier spectrum in the previous section. During the pulse, there is visible nonadiabatic character for field energies of 1.55 and 2.00 eV; the dipole moment response appears to be adiabatic during the pulse for the field energy of 3.00 eV.

Fourier analysis of the residual dipole moment oscillations is shown in Figure 15. Each of the excited-state energies labeled in the figure corresponds to an excited-state calculated by linear response TDHF that has a transition dipole parallel to the applied electric field. As the field frequency increases, the height of the 1.51 eV peak decreases, and that of the peaks at 3.3, 4.5, and 7.1 eV increases. When the applied field energy reaches 3.00 eV, new peaks appear corresponding to energies of 6.6 and 8.7 eV. The increase in the excitation volume of the higher-energy excited-states is much more evident for anthracene 1+. Figures 16 and 17 show the dipole moment response for

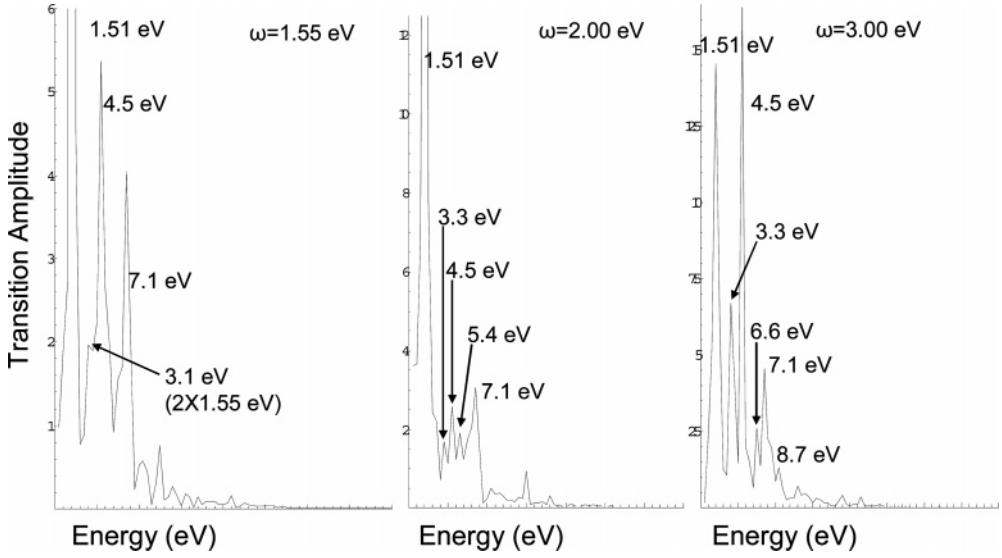

Figure 15. The Fourier transform of the residual dipole moment oscillations of naphthalene 1+ at the neutral geometry for electric field frequencies of 1.55, 2.00, and 3.00 eV for $\mathbf{E}_{max} = 0.0155$ au. (Note: the scale of the left panel is $^1/_2$ the scale of the other two panels).

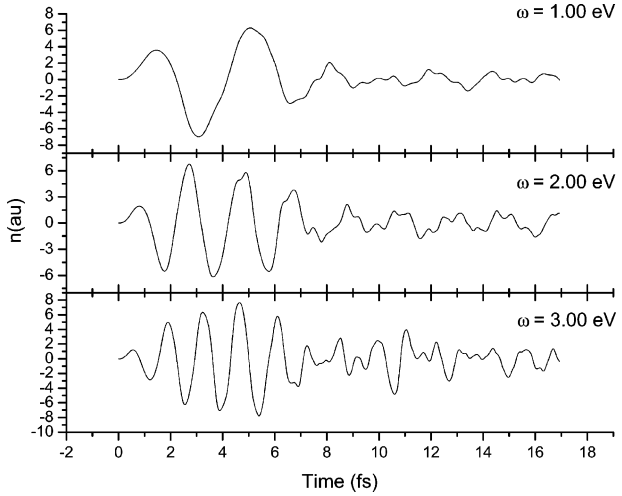

Figure 16. The dipole response of the anthracene 1+ cation at the neutral geometry for electric field frequencies of 1.00, 2.00, and 3.00 eV for $\mathbf{E}_{max} = 0.0184$ au.

anthracene 1+ at the neutral geometry at field frequencies of 1.00, 2.00, and 3.00 eV at a maximum field intensity of 0.0184 au. From Figure 16 it is evident that there is increasing nonadiabatic character as the frequency of the laser field is increased, whereas Figure 17 shows the increase in excitation volume and transitions to higher-energy states as field energy increases.

The frequency response of the dipole moment for the mono cations of naphthalene and anthracene suggests the following two main points: (i) with increasing frequency, excitation volume increases; and (ii) the excited-state populations move to higher-energy excited-states with higher frequency excitation. The increase in excitation can be explained qualitatively using Dykhne-type theories. Increasing the frequency increases the excitation probability. However, this two-state theory cannot fully account for the multistate systems studied here. Thus, the shift of excited-state volumes to higher-energy states may possibly be explained by a combination of Dykhne-type transitions between the excited-states. Field free excited-state calculations for naphthalene monocation and anthracene monocation using the configuration interaction with singles excitations (CIS) level of theory show that, for some transitions between excited-states, the transition dipoles are parallel to the applied field. Several of the higher-energy peaks in Figures 15 and 17 can arise from excited-state to excited-state transitions because the transition dipole moments are parallel to the field and energies for these transitions are either single or integer multiples of the applied field energy. Increasing the field frequency may bring more of these transitions nearer to either single- or multiphoton resonance.

IV. Conclusion

In this paper, we have used TDHF theory to simulate the interaction of an intense laser field with a series of polyacenes of increasing length and conjugation. The neutral, 1+, and 2+ cations of benzene, naphthalene, anthracene, and tetracene were examined. The field was aligned along the long axis of the molecule at laser intensities that correspond to negligible ionization probability. The time evolution of the dipole moment, Löwden charges, and occupation numbers were used to determine the nonadiabatic effects of the electric field on these polyacenes. For each molecule, the nonadiabatic response was evident in the residual dipole moment oscillations with the greatest degree seen for the monocations. The response of the dipole moment reveals that the lowest energy excited-state with a transition dipole parallel to the applied field is the most strongly coupled to the field, which is in agreement with the model theory of ref 27. As the size and conjugation of the molecules increase, geometry optimization for the ion has less effect on the response of the amplitude of the residual dipole moment oscillations. For cations of benzene and naphthalene, the excited-state energy at the neutral geometry was slightly lower, explaining the increased coupling to the applied field.

The dependence of the electron dynamics for naphthalene and anthracene monocations (at the neutral geometry) on the field intensity was studied using three values of intensity for each molecule. As the intensity increased, the Fourier coefficients for the most strongly coupled state and lower-energy excited-states decrease while the coefficients for higher-energy excited-states increase. This suggests that population was transferred from lower-energy excited-states to higher-energy excited-states as the intensity increased.

The frequency dependence of the electron dynamics for naphthalene 1+ and anthracene 1+, both at the neutral geometry, was examined at three field frequencies for each molecule. The excited-state spectrum changes significantly for increasing field frequency. As the field frequency increases, the Fourier coefficients for the lower-energy excited-states decrease, and the coefficients for higher-energy excited-states increase significantly. Thus, increasing the field frequency increases the

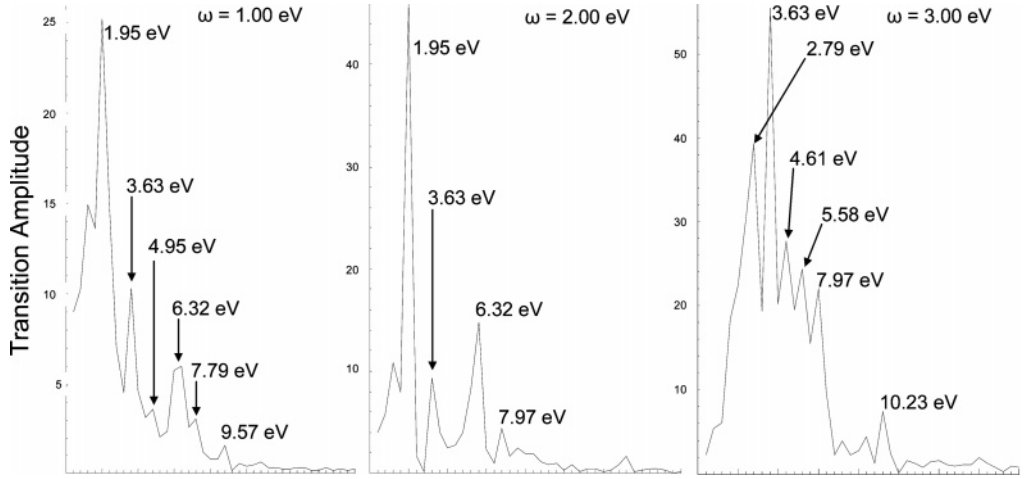

Figure 17. The Fourier transform of the residual dipole moment oscillations of anthracene 1+ at the neutral geometry for electric field frequencies of 1.00, 2.00, and 3.00 eV for $\mathbf{E}_{max} = 0.0184$ au. (Note: the transition amplitude scale is different for each panel.)

excitation volume and moves the volume toward higher-energy excited-states in accordance with Landau−Zener and Dykhne theories.

Acknowledgment. This work was supported by grants from the National Science Foundation CHE No. 0512144 (H.B.S) and No. 331390111 (R.J.L), Defense Advanced Research Projects Agency No. 311390111 (R.J.L), and the Army Research Office No. 311390121 (R.J.L).

References and Notes

(1) Wang, B.; Halbhuber, K.-J.; Riemann, I.; Koenig, K. *Proc. SPIE - Int. Soc. Opt. Eng.* **2005**, *5964*, 59640O/1.
(2) Tan, H.-Y.; Sun, Y.; Lo, W.; Lin, S.-J.; Hsiao, C.-H.; Chen, Y.-F.; Huang Samuel, C.-M.; Lin, W.-C.; Jee, S.-H.; Yu, H.-S.; Dong, C.-Y. *Invest. Ophthalmol. Visual Sci.* **2006**, *47*, 5251.
(3) Ding, D.; Huang, J.; Compton, R. N.; Klots, C. E.; Haufler, R. E. *Phys. Rev. Lett.* **1994**, *73*, 1084.
(4) Ding, D.; Compton, R. N.; Haufler, R. E.; Klots, C. E. *J. Phys. Chem.* **1993**, *97*, 2500.
(5) Baev, A.; Rubio-Pons, O.; Gel'mukhanov, F.; Agren, H. *J. Phys. Chem. A* **2004**, *108*, 7406.
(6) Tsubouchi, M.; Whitaker, B. J.; Suzuki, T. *J. Phys. Chem. A* **2004**, *108*, 6823.
(7) Yoo, H. S.; DeWitt, M. J.; Pate, B. H. *J. Phys. Chem. A* **2004**, *108*, 1365.
(8) Barker, J. R.; Yoder, L. M.; King, K. D. *J. Phys. Chem. A* **2001**, *105*, 796.
(9) He, Y. B.; Pochert, J.; Quack, M.; Ranz, R.; Seyfang, G. *Faraday Discuss.* 1995, 275.
(10) Che, J. W.; Krause, J. L.; Messina, M.; Wilson, K. R.; Yan, Y. J. *J. Phys. Chem.* **1995**, *99*, 14949.
(11) Shapiro, M.; Brumer, P. *J. Chem. Phys.* **1993**, *98*, 201.
(12) Leite, S. R. D.; Isolani, P. C.; Riveros, J. M. *Can. J. Chem.* **1984**, *62*, 1380.
(13) Keldysh, L. V. *Sov. Phys. JTEP* **1965**, *20*, 1307.
(14) Ammosov, M. V.; Delone, N. B.; Krainov, V. P. *Sov. Phys. JTEP* **1986**, *81*, 5101.
(15) DeWitt, M. J.; Levis, R. J. *J. Chem. Phys.* **1999**, *110*, 11368.
(16) DeWitt, M. J.; Levis, R. J. *Phys. Rev. Lett.* **1998**, *81*, 5101.
(17) Muller, H. G.; Bucksbaum, P. H.; Schumacher, D. W.; Zavriyev, A. *J. Phys. B* **1990**, *23*, 2761.
(18) Muller, H. G. *Phys. Rev. A* **1999**, *60*, 1341.
(19) Eberly, J. H.; Javanainen, J.; Rzazewski, K. *Phys. Rep.* **1991**, *204*, 331.
(20) Zuo, T.; Bandrauk, A. D. *J. Nonlinear Opt. Phys. Mater.* **1995**, *4*, 533.
(21) McPherson, A.; Gibson, G.; Jara, H.; Johann, U.; Luk, T. S.; McIntyre, I. A.; Boyer, K.; Rhodes, C. K. *J. Opt. Soc. Am. B* **1987**, *4*, 595.
(22) Lhuillier, A.; Schafer, K. J.; Kulander, K. C. *J. Phys. B* **1991**, *24*, 3315.
(23) Salieres, P.; Antoine, P.; de Bohan, A.; Lewenstein, M. *Phys. Rev. Lett.* **1998**, *81*, 5544.
(24) Antoine, P.; Lhuillier, A.; Lewenstein, M. *Phys. Rev. Lett.* **1996**, *77*, 1234.
(25) Lezius, M.; Blanchet, V.; Rayner, D. M.; Villeneuve, D. M.; Stolow, A.; Ivanov, M. Y. *Phys. Rev. Lett.* **2001**, *86*, 51.
(26) Lezius, M.; Blanchet, V.; Ivanov, M. Y.; Stolow, A. *J. Chem. Phys.* **2002**, *117*, 1575.
(27) Markevitch, A. N.; Smith, S. M.; Romanov, D. A.; Schlegel, H. B.; Ivanov, M. Y.; Levis, R. J. *Phys. Rev. A* **2003**, *68*, 011402(R).
(28) Markevitch, A. N.; Romanov, D. A.; Smith, S. M.; Schlegel, H. B.; Ivanov, M. Y.; Levis, R. J. *Phys. Rev. A* **2004**, *69*, 013401.
(29) Bucksbaum, P. H.; Zavriyev, A.; Muller, H. G.; Schumacher, D. W. *Phys. Rev. Lett.* **1990**, *64*, 1883.
(30) Zavriyev, A.; Bucksbaum, P. H.; Muller, H. G.; Schumacher, D. W. *Phys. Rev. A* **1990**, *42*, 5500.
(31) Frasinski, L. J.; Posthumus, J. H.; Plumridge, J.; Codling, K.; Taday, P. F.; Langley, A. J. *Phys. Rev. Lett.* **1999**, *83*, 3625.
(32) Seideman, T.; Ivanov, M. Y.; Corkum, P. B. *Phys. Rev. Lett.* **1995**, *75*, 2819.
(33) Zuo, T.; Bandrauk, A. D. *Phys. Rev. A* **1995**, *52*, R2511.
(34) Cornaggia, C.; Lavancier, J.; Normand, D.; Morellec, J.; Agostini, P.; Chambaret, J. P.; Antonetti, A. *Phys. Rev. A* **1991**, *44*, 4499.
(35) Cornaggia, C.; Schmidt, M.; Normand, D. Coulomb *J. Phys. B* **1994**, *27*, L123.
(36) Bhardwaj, V. R.; Corkum, P. B.; Rayner, D. M. *Phys. Rev. Lett.* **2003**, *91*, No. 203004.
(37) Markevitch, A. N.; Romanov, D. A.; Smith, S. M.; Levis, R. J. *Phys. Rev. Lett.* **2004**, *92*, No. 063001.
(38) Faisal, F. H. M. *J. Phys. B* **1973**, *8*, L89.
(39) Reiss, H. R. *Phys. Rev. A* **1980**, *22*, 1786.
(40) Perelomov, A. M.; Popov, S. V.; Terent'ev, M. V. *Sov. Phys. JTEP* **1966**, *23*, 924.
(41) Tong, X. M.; Zhao, Z. X.; Lin, C. D. *Phys. Rev. A* **2002**, *66*, No. 033402.
(42) DeWitt, M. J.; Levis, R. J. *J. Chem. Phys.* **1998**, *108*, 7045.
(43) DeWitt, M. J.; Levis, R. J. *J. Chem. Phys.* **1998**, *108*, 7739.
(44) Tchaplyguine, M.; Hoffmann, K.; Duhr, O.; Hohmann, H.; Korn, G.; Rottke, H.; Wittmann, M.; Hertel, I. V.; Campbell, E. E. B. *J. Chem. Phys.* **2000**, *112*, 2781.
(45) von Helden, G.; Holleman, I.; Knippels, G. M. H.; van der Meer, A. F. G.; Meijer, G. *Phys. Rev. Lett.* **1997**, *79*, 5234.
(46) Muth-Bohm, J.; Becker, A.; Chin, S. L.; Faisal, F. H. M. *Chem. Phys. Lett.* **2001**, *337*, 313.
(47) Schulz, M.; Tretiak, S.; Chernyak, V.; Mukamel, S. *J. Am. Chem. Soc.* **2000**, *122*, 452.
(48) Tretiak, S.; Chernyak, V.; Mukamel, S. *Phys. Rev. Lett.* **1996**, *77*, 4656.
(49) Tretiak, S.; Chernyak, V.; Mukamel, S. *Chem. Phys. Lett.* **1996**, *259*, 55.
(50) Meier, T.; Mukamel, S. *Phys. Rev. Lett.* **1996**, *77*, 3471.
(51) Shanker, B.; Applequist, J. *J. Phys. Chem.* **1996**, *100*, 10834.
(52) Chen, G. H.; Mukamel, S. *J. Phys. Chem.* **1996**, *100*, 11080.
(53) Kirtman, B.; Toto, J. L.; Robins, K. A.; Hasan, M. *J. Chem. Phys.* **1995**, *102*, 5350.
(54) Smith, S. M.; Markevitch, A. N.; Romanov, D. A.; Li, X. S.; Levis, R. J.; Schlegel, H. B. *J. Phys. Chem. A* **2004**, *108*, 11063.
(55) Ingamells, V. E.; Papadopoulos, M. G.; Raptis, S. G. *Chem. Phys. Lett.* **1999**, *307*, 484.
(56) Rozyczko, P. B.; Bartlett, R. J. *J. Chem. Phys.* **1998**, *108*, 7988.
(57) Oliveira, L. N.; Amaral, O. A. V.; Castro, M. A.; Fonseca, T. L. *Chem. Phys.* **2003**, *289*, 221.
(58) Harumiya, K.; Kono, H.; Fujimura, Y.; Kawata, I.; Bandrauk, A. D. *Phys. Rev. A* **2002**, *66*, art. no. 043403.
(59) Walsh, T. D. G.; Ilkov, F. A.; Chin, S. L.; Chateauneuf, F.; Nguyen-Dang, T. T.; Chelkowski, S.; Bandrauk, A. D.; Atabek, O. *Phys. Rev. A* **1998**, *58*, 3922.
(60) Yu, H. T.; Zuo, T.; Bandrauk, A. D. *Phys. Rev. A* **1996**, *54*, 3290.
(61) Talebpour, A.; Vijayalakshmi, K.; Bandrauk, A. D.; Nguyen-Dang, T. T.; Chin, S. L. *Phys. Rev. A* **2000**, *62*, No. 042708.
(62) Lein, M.; Kreibich, T.; Gross, E. K. U.; Engel, V. *Phys. Rev. A* **2002**, *65*, No. 033403.
(63) Kawata, I.; Bandrauk, A. D.; Kono, H.; Fujimura, Y. *Laser Phys.* **2001**, *11*, 188.
(64) Bandrauk, A. D.; Chelkowski, S. *Phys. Rev. Lett.* **2000**, *84*, 3562.
(65) Bandrauk, A. D.; Chelkowski, S.; Zamojski, M. *Z. Phys. Chem. Int. J. Res. Phys. Chem., Chem. Phys.* **2000**, *214*, 1393.
(66) Bandrauk, A. D.; Lu, H. Z. *Phys. Rev. A* **2000**, *62*.
(67) Suzuki, M.; Mukamel, S. *J. Chem. Phys.* **2003**, *119*, 4722.
(68) Suzuki, M.; Mukamel, S. *J. Chem. Phys.* **2004**, *120*, 669.
(69) Chu, S. I. *J. Chem. Phys.* **2005**, *123*, 62207.
(70) Chu, S. I.; Telnov, D. A. *Phys. Rep.* **2004**, *390*, 1.
(71) Chu, X.; Chu, S.-I. *Phys. Rev. A* **2004**, *70*, 061402.
(72) Guan, X. X.; Tong, X. M.; Chu, S. I. *Phys. Rev. A* **2006**, *73*, 23403.
(73) Telnov, D. A.; Chu, S. I. *Phys. Rev. A* **2005**, *71*, 13408.
(74) Usachenko, V. I.; Chu, S. I. *Phys. Rev. A* **2005**, *71*, 63410.
(75) Usachenko, V. I.; Pyak, P. E.; Chu, S. I. *Laser Phys.* **2006**, *16*, 1326.
(76) Nest, M.; Klamroth, T.; Saalfrank, P. *J. Chem. Phys.* **2005**, *122*, 124102.
(77) Krause, P.; Klamroth, T.; Saalfrank, P. *J. Chem. Phys.* **2005**, *123*, 074105.
(78) Klamroth, T. N-methyl-6-quinolone. *J. Chem. Phys.* **2006**, *124*, 20517879.
(79) Schlegel, H. B.; Smith, S. M.; Li, X. *J. Chem. Phys.*, **2007**, *126*, 244110.
(80) Kuleff, A. I.; Breidbach, J.; Cederbaum, L. S. *J. Chem. Phys.* **2005**, *123*, 044111.
(81) Hennig, H.; Breidbach, J.; Cederbaum, L. S. *J. Phys. Chem. A* **2005**, *109*, 409.
(82) Li, X. S.; Smith, S. M.; Markevitch, A. N.; Romanov, D. A.; Levis, R. J.; Schlegel, H. B. *Phys. Chem. Chem. Phys.* **2005**, *7*, 233.
(83) Smith, S. M.; Li, X. S.; Markevitch, A. N.; Romanov, D. A.; Levis, R. J.; Schlegel, H. B. *J. Phys Chem A* **2005**, *109*, 5176.
(84) Smith, S. M.; Li, X. S.; Markevitch, A. N.; Romanov, D. A.; Levis, R. J.; Schlegel, H. B. *J. Phys. Chem. A* **2005**, *109*, 10527.
(85) Kulander, K. C. *Phys. Rev. A* **1987**, *36*, 2726.
(86) Kulander, K. C. *Phys. Rev. A* **1987**, *35*, 445.
(87) Tsiper, E. V.; Chernyak, V.; Tretiak, S.; Mukamel, S. *Chem. Phys. Lett.* **1999**, *302*, 77.
(88) Micha, D. A. *J. Phys. Chem. A* **1999**, *103*, 7562.

(89) Micha, D. A. Density Matrix Treatment of Electronic Rearrangement. In *Advances in Quantum Chemistry* Academic Press: San Diego, 1999; Vol. 35, pp 317.

(90) *Atomic and Molecular Processes with Short Intense Laser Pulses*; Bandrauk, A. D., Ed.; Springer: New York, 1988.

(91) *Coherence Phenomena in Atoms and Molecules in Laser Fields*; Bandrauk, A. D., Wallace, S. C., Eds.; Springer: New York, 1992.

(92) *Molecules in Laser Fields*; Bandrauk, A. D., Ed.; Marcel Dekker, Inc.: New York, 1993.

(93) Frisch, M. J.; Trucks, G. W..; Schlegel, H. B.; Scuseria, G. E.; Robb, M. A.; Cheeseman, J. R.; Montgomery, J. A., Jr.; Vreven, T.; Kudin, K. N.; Burant, J. C.; Millam, J. M.; Iyengar, S. S.; Tomasi, J.; Barone, V.; Mennucci, B.; Cossi, M.; Scalmani, G.; Rega, N.; Petersson, G. A.; Nakatsuji, H.; Hada, M.; Ehara, M.; Toyota, K.; Fukuda, R.; Hasegawa, J.; Ishida, M.; Nakajima, T.; Honda, Y.; Kitao, O.; Nakai, H.; Klene, M.; Li, X.; Knox, J. E.; Hratchian, H. P.; Cross, J. B.; Bakken, V.; Adamo, C.; Jaramillo, J.; Gomperts, R.; Stratmann, R. E.; Yazyev, O.; Austin, A. J.; Cammi, R.; Pomelli, C.; Ochterski, J. W.; Ayala, P. Y.; Morokuma, K.; Voth, G. A.; Salvador, P.; Dannenberg, J. J.; Zakrzewski, V. G.; Dapprich, S.; Daniels, A. D.; Strain, M. C.; Farkas, O.; Malick, D. K.; Rabuck, A. D.; Raghavachari, K.; Foresman, J. B.; Ortiz, J. V.; Cui, Q.; Baboul, A. G.; Clifford, S.; Cioslowski, J.; Stefanov, B. B.; Liu, G.; Liashenko, A.; Piskorz, P.; Komaromi, I.; Martin, R. L.; Fox, D. J.; Keith, T.; Al-Laham, M. A.; Peng, C. Y.; Nanayakkara, A.; Challacombe, M.; Gill, P. M. W.; Johnson, B.; Chen, W.; Wong, M. W.; Gonzalez, C.; Pople, J. A. *Gaussian 03*, Revision d.01; Gaussian, Inc.: Wallingford, CT, 2004.

(94) Li, X. S.; Tully, J. C.; Schlegel, H. B. *J. Chem. Phys.* **2005**, *123*, 084106.

(95) Corkum, P. B. *Phys. Rev. Lett.* **1993**, *71*, 1994.

(96) Bhardwaj, V. R.; Rayner, D. M.; Villeneuve, D. M.; Corkum, P. B. *Phys. Rev. Lett.* **2001**, *87*, 253003.

(97) Smits, M.; de Lange, C. A.; Stolow, A.; Rayner, D. M. *Phys. Rev. Lett*. **2004**, *93*, 203402.

(98) Talebpour, A.; Larochelle, S.; Chin, S. L. *J. Phys. B* **1998**, *31*, 2769.

(99) Zhao, Z. X.; Brabec, T. *J. Phys. B* **2006**, *39*, L345.

(100) Brabec, T.; Cote, M.; Boulanger, P.; Ramunno, L. *Phys. Rev. Lett.* **2005**, *95*, 073001.

(101) Delone, N. B.; Krainov, V. P. *Atoms in Strong Laser Fields*; Springer-Verlag: Berlin, 1985.

(102) Smith, S. M.; Markevitch, A. N.; Romanov, D. A.; Li, X.; Levis, R. J.; Schlegel, H. B. *J. Phys. Chem. A* **2004**, *108*, 11063.